DEVELOPMENT OF AN ENHANCED ACTUATOR DISC MODEL FOR THE SIMULATION OF WIND FARMS

Asif Zubair

asif.zubair@tecnico.ulisboa.pt

Instituto Superior Técnico, Universidade de Lisboa, Portugal

November 2016

Abstract

CFD is one of many tools available to predict the performance and flow characteristics of a horizontal axis wind turbine. CFD simulations of a fully resolved 3D turbine geometry gives good results but it is computationally very demanding in terms of time and computational power. An alternate approach is to use a simplified CFD-BEMT approach in which the turbine is reduced to a so called actuator disc and coupled to Blade Element Momentum Theory (BEMT). Wind turbine blades generate vortices at the tip region due to difference in pressure between upper and lower surface of the blade. These tip vortices reduce the lift and hence efficiency, particularly near the tip region. CFD-BEMT model is not capable to take into account the effect of tip vortices on the performance as well as in the flow field. In this article, three enhanced actuator disc models are presented which are developed by combining BEMT with Lifting Line Theory (LLT) and coupling them to CFD. The three methods use different approaches to combine BEMT with LLT. Simulations are performed for CFD-BEMT, with and without the Prandtl tip loss effect, and with the three enhanced actuator disc models and results are produced for the performance of turbine as well as for the flow field. Performance results from all these models are compared with the results obtained from FAST V8 commercial code and flow field results are compared with the results obtained from LLT IST code.

Keywords: CFD, Blade Element Momentum Theory, actuator disc, Lifting Line Theory, tip vortices

1. Introduction:

The wind turbines generate downstream wakes. When wind turbines are arranged in a wind farm with limited area, power losses occur due to turbine wake interference [10]. Field experiments and computational fluid dynamics (CFD) have unanimously shown that the power produced by a wind farm is lower than the combined rated powers of its constituent turbines. This is because a wind turbine extracts energy from freestream atmospheric flow. This generates wake at the downstream side of turbine with reduced velocity. This wake interacts with a downstream wind turbine and limits its power generation capacity [8]. To minimize wake losses, optimization of wind farm layout is required. The optimization of a wind farm layout in turn depends on the accurate modelling of the wind turbine performance as well as the flow field around and downstream of a wind turbine.

CFD simulations have the potential to predict the aerodynamics characteristics of a wind turbine as well as the flow field characteristics around the turbine and in the wake region. However, simulating the flow around a fully resolved 3D horizontal axis wind turbine (HAWT) geometry requires high computational power and time. An alternate approach is to use a simplified and mixed CFD-BEMT approach which requires less computational power and time [2][4]. BEMT assumes an infinite number of blades and, as a consequence,

considers that the forces acting on the rotor are distributed over the complete rotor disc surface [5]. In reality, a wind turbine has a finite number of blades. As a result, flow slippage occurs at the tip of the blades from the pressure side to suction side of the blade due to the pressure difference. This flow slippage is responsible for generating tip vortices as described in [9]. The flow slippage reduces the forces as well as the power production capability along the blade and particularly at the tip region. This effect is known as the tip loss effect [7]. The CFD-BEMT model does not capture the effect of tip vortices and therefore it has two major shortcomings; it over predicts the performance and it generates unrealistic flowfields. In the simple BEMT, the tip loss effect can be introduced via some empirical tip loss model. An example of such a tip loss model is the Prandtl tip loss factor. The implementation of the Prandtl tip loss factor reduces the forces acting along the turbine blade. The reduction in force is high near the tip where the tip vortices have a pronounced effect [7]. When the Prandtl tip loss model is applied in BEMT-CFD, it reduces the reactive forces exerted by the blades on the fluid and as a result, the fluid passes through the turbine with little momentum change at the tip when the actuator disc model is implemented in the CFD model. Hence the effect of the tip vortices is still not captured in a CFD-BEMT coupling with the Prandtl tip loss model and the flow field prediction is unrealistic [3].

For the simulation of wind farms, an accurate prediction of performance and downstream flow field of a wind turbine are required. Hence BEM-CFD models, with or without tip loss correction factor, are not suitable for the simulation of wind farms and there is a need to develop a more sophisticated CFD model capable of accurately predicting both the performance as well as the downstream flow field in the wake of a wind turbine.

In this article three “enhanced actuator disc models“ for CFD are presented. These models are developed by combining BEMT with LLT and coupling them to the simple actuator disc concept in CFD. CFD simulations are performed for CFD-BEMT with and without tip loss, and with the three enhanced actuator disc models. The simulation results are compared with each other and with the results obtained from FAST V8, which is an open source software developed by NREL for the design and analysis of wind turbines, and the LLT IST code, which is a software developed in Instituto Superior Técnico (IST), Lisbon that uses Lifting Line theory to predict the aerodynamic characteristics of a wind turbine.

2. Numerical Models:

The method is based on the solution of the Reynolds-Averaged Navier Stokes (RANS) equations in combination with the BEMT.

2.1 The RANS equations:

Simulations were performed using ANSYS CFX with the Reynolds-Averaged Navier Stokes (RANS) equations which are obtained by averaging the fluctuating quantities in the original transport equations. In the following steady-state RANS equations, the bar is dropped for averaged quantities, except for products of fluctuating quantities. The continuity and momentum equations are given as:

$$\frac{\partial}{\partial x_j}\rho(U_j) = 0 \tag{1}$$

$$\frac{\partial}{\partial x_j}\rho(U_i U_j) = -\frac{\partial p}{\partial x_i} + \frac{\partial}{\partial x_i}(\tau_{ij} - \rho\overline{U_i U_j}) + S_i \tag{2}$$

Where ρ is the density, U_i $(i = u,v,w)$ is the averaged velocity, x_i $(i = x, y, z)$ is the position, p is the mean pressure, τ is the molecular stress tensor, $\rho\overline{U_i U_j}$ are the Reynolds stresses, and S_i are additional source terms in the $i = x, y, z$ momentum equations. The

Reynolds stresses were calculated from the k-ω SST model.

2.2 The CFD-BEMT model:

In BEMT, the effect of multiple airfoils (blades) is averaged over one complete rotation. In CFD-

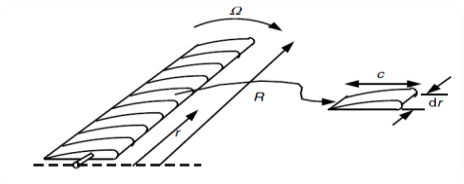

Figure 1: Schematics of blade elements

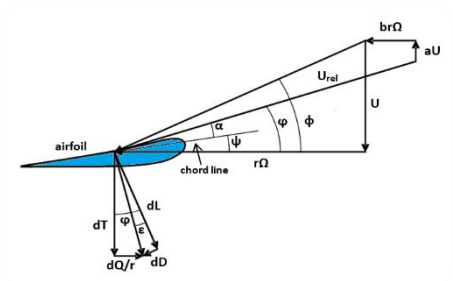

Figure 2: forces on a blade section

BEMT model, the effect of blades on the fluid is introduced through momentum source terms in the Navier-Stokes equations (see Equation(2)). BEMT discretizes the blade in a number of elements as shown in Figure 1. The forces on each blade section are as shown in the Figure 2.

The induced flow inclination angle is defined as

$$\varphi = \tan^{-1}\frac{U(1-a)}{\Omega r(1+b)} \qquad (3)$$

where U is undisturbed wind velocity, Ω is angular velocity of turbine, r is the radius of blade element, a is the axial induction factor and b is the tangential induction factor. In the CFD-BEMT model, a and b are calculated from the RANS calculations of the flow field in each iteration with BEMT. The relative velocity of the wind is defined as:

$$U_{rel}^2 = [U(1-a)]^2 + [\Omega r(1+b)]^2 \qquad (4)$$

The lift force, L, and drag force, D, on a blade element are given by:

$$dL = 0.5\rho U_{rel}^2 C_L c dr \qquad (5)$$

$$dD = 0.5\rho U_{rel}^2 C_D c dr \qquad (6)$$

where ρ is the density of air, U_{rel} is the relative velocity of air, C_L is the lift coefficient and C_D is the drag coefficient and c is the chord length. Using Figure 2, the lift and drag forces are related to the axial and tangential forces as follows.

$$dA = dL\cos\varphi + dD\sin\varphi \qquad (7)$$

$$dT = dL\sin\varphi - dD\cos\varphi \qquad (8)$$

Substituting Equations (5) and (6) into Equations (7) and (8), it gives

$$dA = 0.5\rho U_{rel}^2 c dr(C_L\cos\varphi + C_D\sin\varphi) \qquad (9)$$

$$dT = 0.5\rho U_{rel}^2 c dr(C_L\sin\varphi - C_D\cos\varphi) \qquad (10)$$

These forces converted to force per unit volume give the axial and tangential source terms, ST_{ax} and ST_{tan} as:

$$ST_{ax} = \frac{BdA}{2\pi r\Delta x dr} \qquad (11)$$

$$dST_{tan} = \frac{BdT}{2\pi r\Delta x dr} \qquad (12)$$

where B is the number of blades and Δx is the thickness of the actuator disc. When the Prandtl tip loss correction is applied, Equations (11) and (12) become:

$$ST_{ax} = \frac{BFdA}{2\pi r\Delta x dr} \qquad (13)$$

$$dST_{tan} = \frac{BFdT}{2\pi r\Delta x dr} \qquad (14)$$

where F is the Prandtl tip loss correction factor defined as:

$$F = \frac{2}{\pi}arc\cos\left(exp\frac{-B(R-r)}{2r\sin\varphi}\right) \qquad (15)$$

2.3 CFD-BEMT+LLT Model

2.3.1 Lifting Line theory

In a wind turbine, vortices are generated at the tip region due to pressure difference between upper and lower surface of the blades. Tip vortices reduce the angle of attack relative to an idealized infinitely

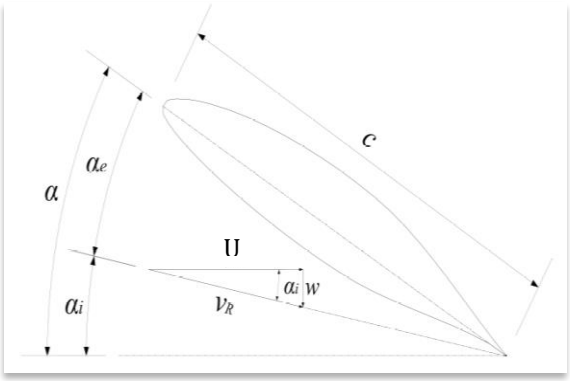

Figure 3: This diagram highlights the components required to define the induced angle of attack [3]

long 2D airfoil which in turn causes reduction in the lift force.

The lift force on a wing is produced due to pressure difference between the lower and upper surfaces of the wing. The associated difference in flow speed above and below the wing section can be characterized as circulation (or vorticity). The induced circulation makes the flow to deflect downwards. This downward deflection is called downwash [3]. According to circulation theory, see [1], the lift force per unit span of a 2D wing of constant section is calculated as:

$$L = \rho U \Gamma \tag{16}$$

Where Γ is the circulation. Figure 3 shows the geometric angle of attack α is composed of two further components; induced angle of attack α_i and the effective angle of attack α_e. The induced angle of attack is the angle of downward deflection resulting from induced downwash [3]. The induced angle of attack can be computed by:

$$\alpha_i = \tan^{-1} w/U \tag{17}$$

The effective angle of attack is given by:

$$\alpha_e = \alpha - \alpha_i \tag{18}$$

The span wise component of air vector on the upper surface is directed from tip to hub, and on the lower surface, the span wise component of velocity is directed from hub to tip. The physical effect of the resultant shear at the trailing edge is the development of a trailing vortex sheet which contains vorticity [3].

Prandtl's classical lifting line theory, as detailed in [9], describes this phenomenon in terms of an infinite number of horseshoe vortices distributed across the wing. Prandtl's classical lifting line theory is an approach that uses this system of horse shoe vortices (bound wing vortices and trailing wing vortices) to determine the forces on the wing. According to the lifting line theory, for a wing of finite length, α_e at the wing tip is constrained as the angle of attack at which lift force reduces to zero. This then influences the distribution of downwash across the span [3]. Hence when LLT is applied to wind turbines, it is capable of predicting the induced velocities generated by the horse shoe vortex system and further calculate the forces on the blades of turbine.

2.3.2 CFD-BEMT+LLT Model

Since wing tip vortices have pronounced effect only in the tip region, in CFD-BEMT+LLT model, LLT is combined with BEM theory only in the last 10% of the blade length near the tip side. From now onwards, this region will be called BEMT+LLT region. In the remaining 90% of the inner blade length, only the BEMT theory is used. From now onwards, this region will be known as the BEMT region.

BEMT region

In CFD-BEMT model discussed earlier, the BEMT was incorporated to the RANS calculations by finding and applying axial and tangential momentum source terms, as shown in Equations (3) to (12). In CFD-BEMT+LLT model, the same procedure is used for CFD-BEMT region as in that region only BEMT is coupled with CFD.

BEMT+LLT region

In BEMT+LLT region, both for axial and tangential directions, two momentum source terms are calculated. They will onwards be referred to as simple momentum source terms and additional

momentum source terms. These two are combined to give cumulative momentum source terms for BEMT+LLT region.

i) Simple Momentum Source Terms

Tip vortices reduce the forces exerted on a blade of finite length as compared to an idealized 2D blade of infinite length. LLT captures the effect of tip vortices on the induced velocities. Simple momentum source terms will impart the effect of reactive forces of the turbine blade on the fluid. In the calculation of simple momentum source terms, induced velocities calculated from LLT are used in the CFD-BEMT model discussed earlier. The result is that, the forces on the blades and hence the momentum source terms are reduced as compared to simple CFD-BEMT model.

The procedure to calculate simple momentum source terms is given here. LLT is used to calculate the axial and tangential induced velocities, v_a and v_t, in the BEMT+LLT region. These induced velocities are used to find the induced flow inclination angle as below:

$$\varphi = \tan^{-1}\frac{U - v_a}{\Omega r + v_t} \tag{19}$$

The relative velocity of the wind is calculated as:

$$U_{rel}^2 = [U - v_a]^2 + [\Omega r + v_t]^2 \tag{20}$$

After finding the flow inclination angle and relative velocity using induced velocities calculated from LLT, simple momentum source terms are calculated using the same procedure and formulations as that of CFD-BEMT model from Equation (5) to (12).

ii) Additional momentum source terms

Additional momentum source terms represent the effect of the tip vortices on the fluid field in terms of induced velocities. The induced velocities calculated by LLT contain the effect of tip vortices. The idea used to calculate the additional momentum source terms is that to calculate the difference in induced velocities (additional induced velocities) from the LLT and the flow field and transform that difference in velocity into a force. Three different approaches, Method 1, Method 2 and Method 3, are used to transform the difference in induced velocity to the force.

a) Method 1 (M1):

Edmunds et al [3] states that the additional reactive force at the tip required to generate the induced velocity for the zero lift condition is given by

$$dF_v = 0.5\rho w_a^2 c dr \tag{21}$$

Where w_a is the additional induced velocity required to achieve zero lift condition at the tip. The same idea is used in this method. The difference in induced velocities from LLT and the RANS calculations are used to calculate the additional reactive force using the formulation above in Equation (21). This additional reactive force is used to calculate the additional momentum source terms by finding a force per unit volume as:

$$AST_{ax} = \frac{BdF_{v_{ax}}}{2\pi r \Delta x dr} = \frac{B\rho\left(v_{a_{LLT}} - v_{a_{RS}}\right)^2 c}{4\pi r \Delta x} \tag{22}$$

$$AST_{tan} = \frac{BdF_{v_{tan}}}{2\pi r \Delta x dr} = \frac{B\rho\left(v_{t_{LLT}} - v_{t_{RS}}\right)^2 c}{4\pi r \Delta x} \tag{23}$$

Where $v_{a_{LLT}}$ and $v_{a_{RS}}$ are the axial induced velocities from LLT and the RANS calculations respectively and $v_{t_{LLT}}$ and $v_{t_{RS}}$ are tangential induced velocities from LLT and the RANS calculations respectively. The source terms calculated from this method are the smallest in magnitude.

b) Method 2 (M2):

This method is based on momentum balance and uses Newton's second Law of motion. The difference in induction velocities from the LLT and the RANS calculations is obtained. This difference is used to calculate the rate of change of momentum required to produce this change of velocity, which is equivalent to force, F_m. The momentum source terms are calculated by finding

the force per unit volume. The axial and tangential source terms for this method are given as

$$AST_{ax} = \frac{dF_{m_{ax}}}{dA_r \Delta x} = \frac{\rho\left(U - v_{a_{RS}}\right)\left(v_{a_{LLT}} - v_{a_{RS}}\right)}{\Delta x} \quad (24)$$

$$AST_{tan} = \frac{dF_{m_{tan}}}{dA_r \Delta x} = \frac{\rho\left(U - v_{a_{RS}}\right)\left(v_{t_{LLT}} - v_{t_{RS}}\right)}{\Delta x} \quad (25)$$

where dA_r is the differential cross section area of control volume. The source terms calculated from M2 are higher than M1 but lower than M2.

c) Method 3 (M3):

This method is identical to Method 2. The only difference is that, induced velocities from the RANS calculations are assumed to be zero in the BEMT+LLT region. Hence, the difference in induced velocities from LLT and the RANS calculations will reduce to the absolute value of induced velocities from the LLT code. This method is developed to observe the effects of increased additional source terms. The axial and tangential source terms for this method are given as

$$AST_{ax} = \frac{dF_{m_{ax}}}{dA_r \Delta x} = \frac{\rho\left(U - v_{a_{RS}}\right)\left(v_{a_{LLT}}\right)}{\Delta x} \quad (26)$$

$$AST_{tan} = \frac{dF_{m_{tan}}}{dA_r \Delta x} = \frac{\rho\left(U - v_{a_{RS}}\right)\left(v_{t_{LLT}}\right)}{\Delta x} \quad (27)$$

The source terms calculated from M3 are the highest.

3. Power and thrust coefficients:

The non-dimensional parameters, the tip speed ratio (TSR), power coefficient (C_P) and thrust coefficient (C_T), for a wind turbine are defined as:

$$TSR = r\Omega/U \quad (28)$$

$$C_P = \frac{\omega Q}{\frac{1}{2}\rho U^3 A_s} = \sum \frac{\omega \delta Q}{\frac{1}{2}\rho U^3 A_s} \quad (29)$$

$$C_T = \frac{A}{\frac{1}{2}\rho U^2 A_s} = \sum \frac{\delta A}{\frac{1}{2}\rho U^2 A_s} \quad (30)$$

Where A_s is the rotor swept area, Q is the torque obtained from the product of the radius and the tangential force (rT) in the BEM-CFD simulation, and A is the axial force acting on the turbine. Thus, the equivalent C_P and C_T are calculated by summation over each element with width dr.

4. Reference Turbine:

For the simulations, turbine specifications of "NREL offshore 5-MW baseline wind turbine" are used. The specifications of the turbine are developed by NREL. This wind turbine is a conventional three-bladed upwind variable-speed variable blade-pitch-to-feather-controlled turbine. The complete details of its properties can be found in [11].

5. Simulation setup:

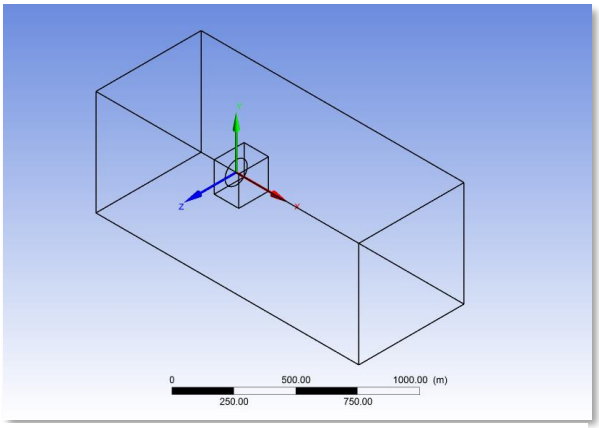

Figure 4: Isometric view of flow domain

Figure 4 shows the fluid domain used for the simulations in ANSYS-CFX. Axial flow is along the x axis and actuator disc is parallel to yz plane. The fluid domain is enclosed by 6 boundaries and contains 3 mesh regions; actuator disc mesh replacing the turbine; fine field mesh region is present around the actuator disc mesh and has a fine mesh resolution; coarse field mesh consists of remaining fluid domain. The fluid used is Air at 25˚C. No turbulence is imparted to incoming air velocity. For all simulations velocity of incoming air is set to 8m/s.

6. Results and Discussion:

6.1 Performance

Figure 5 represents the variation of the power coefficeient with the TSR. FAST BEMT and CFD BEMT predicts higher C_P throughout the range of

TSRs provided which is expected. C_P predicted from the three enhanced actuator disc models show good correlation with each other from TSR = 4 to

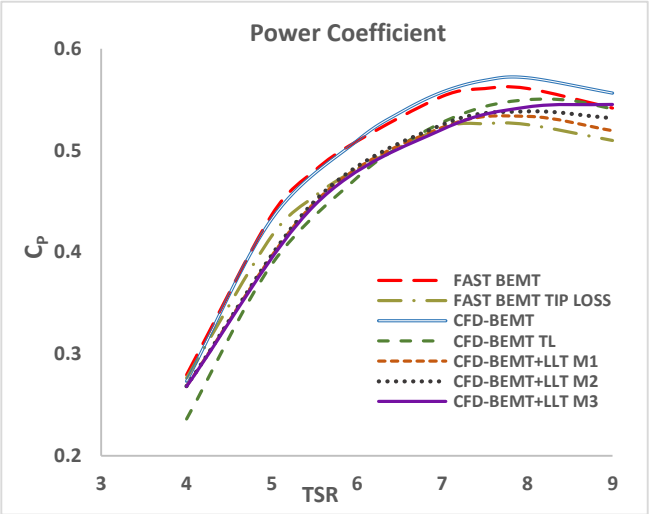

Figure 5: Variation of power coefficient with TSR

TSR = 7. Above TSR = 7, the C_P predicted from these models start to deviate from each other. All enhanced actuator disc models over predict C_P as compared to FAST BEMT Tip loss above TSR =7. CFD-BEMT Prandtl under predicts C_P as compared to FAST BEMT tip loss at low TSR range and over predicts C_P as compared to FAST BEMT tip loss at the high TSR range.

As shown in Figure 6, the C_T predicted from all CFD models increases with increase in the TSR. At high TSRs thrust loading increase and hence C_T increases. CFD-BEMT+LLT M3 and CFD-BEMT+LLT M2 models over predict C_T even as

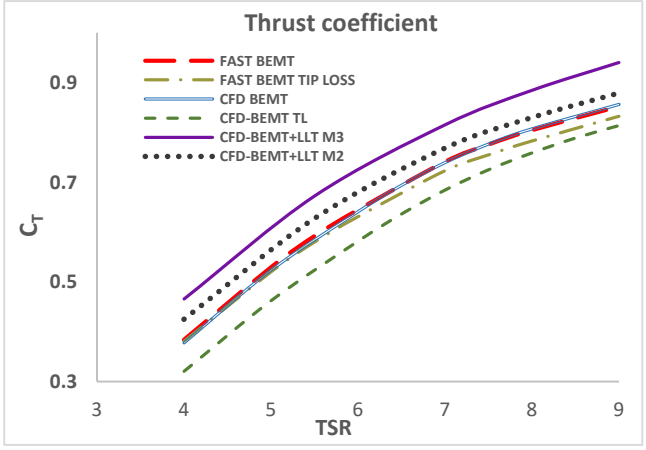

Figure 6: Variation of thrust coefficient with TSR

compared to FAST BEMT and CFD BEMT throughout the TSR range presented because of the high axial additional momentum source terms. CFD-BEMT TL shows the lowest C_T throughout the range of TSR presented because of reduced forces on the blades which produce momentum source terms of low magnitudes.

6.2 Local flow field parameters:

6.2.1 Axial induction factor:

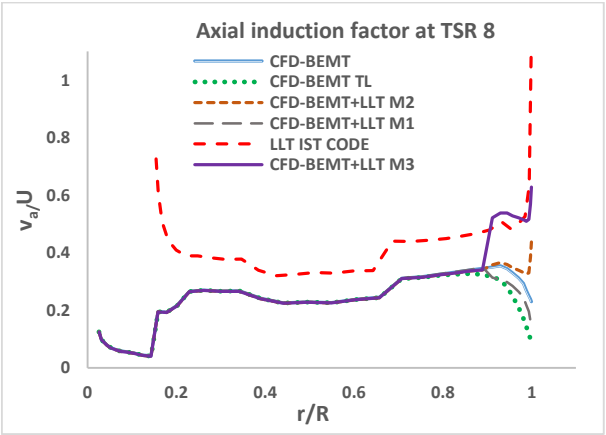

Figure 7: Variation of axial induction factor with dimensionless radial location at TSR = 8

Figure 7 represents the variation of axial induction factor with the dimensionless radial location along the blade. Generally, all CFD models under predict axial induction factors (AIFs) as compared to LLT IST code. CFD-BEMT+LLT M3 model over predicts AIF as compared to LLT IST in the most part of the tip region except at the very tip end. CFD-BEMT+LLT M3 has the highest additional momentum source terms. Therefore, it has higher AIFs in the tip region. CFD-BEMT+LLT M1 has the lowest additional momentum source terms which do not effect much the tip region. Hence AIFs predicted from CFD-BEMT+LLT M1 method are poorer than AIFs predicted from CFD-BEMT. CFD-BEMT TL has the lowest AIFs in the tip region as the tip loss reduces the forces, momentum source terms and hence AIFs in the tip region.

6.2.2 Angle of attack:

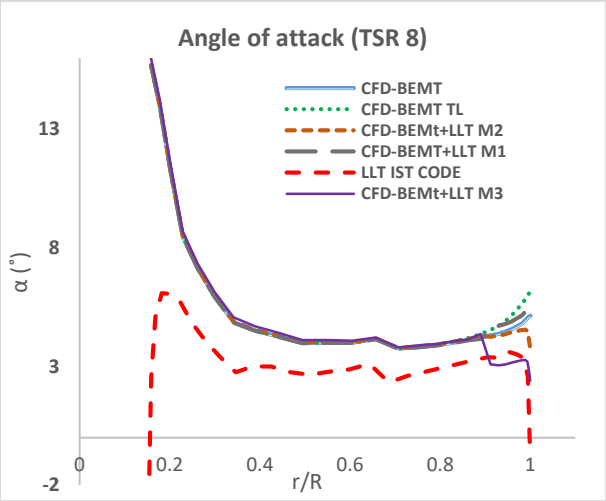

Figure 8: Variation of angle of attack with dimensionless radial location at TSR=8

Figure 8 represents variation of angle of attack (α) with dimensionless radial location along the length of blade at TSR = 8. Generally, all CFD models over predict α as compared to α predicted from LLT IST code throughout the length of blade. LLT IST code shows a sharp decrease in α near the tip in order to achieve the zero lift condition. The same behavior is intended to be incorporated in the enhanced actuator disc models via additional momentum source terms. Clearly, the prediction of α improved in the tip region with CFD-BEMT+LLT M2 and CFD-BEMT+LLT M3 models. Near the tip region, CFD-BEMT+LLT M3 model, with additional momentum source terms of highest magnitudes, follow the trend of predictions from LLT IST code to the highest degree. Yet, at the very tip end, it is not capable of predicting such low values of α as predicted by the LLT IST code. The BEMT+LLT M1 model has additional momentum source terms of lowest magnitudes and hence the prediction from this method is poorer as compared to prediction from CFD-BEMT model. CFD-BEMT TL shows the highest α in the tip region because the tip loss effect reduces the forces and hence the momentum source terms. This generates low axial induced velocities and hence a higher α.

6.3 Axial velocity field

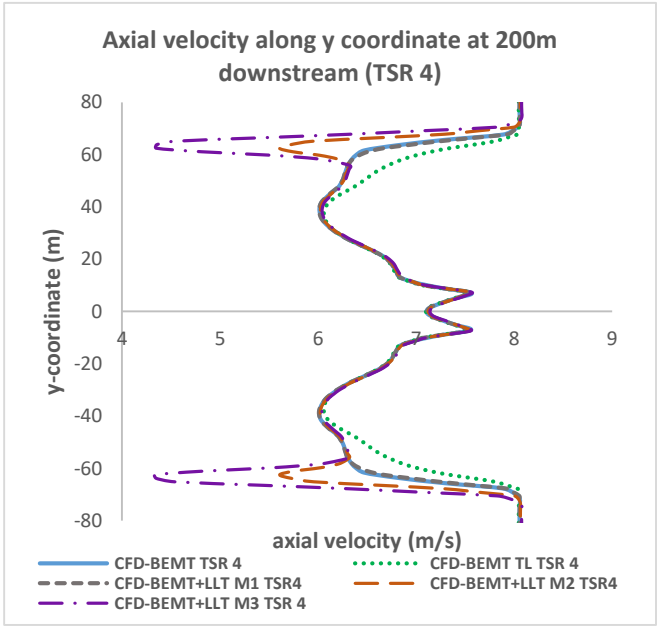

Figure 9: Variation of axial velocity along the y-coordinate at z=0 and at 200 m downstream of wind turbine

Figure 9 shows for TSR 4, the variation of axial velocity along the y coordinate at z = 0 and at 200 m downstream of wind turbine. Clearly the axial additional momentum source terms have reduced the axial velocities significantly in the tip region of the wake for CFD-BEMT+LLT M3 and CFD-BEMT+LLT M2 models. CFD-BEMT+LLT M1 model has axial additional momentum source terms of smallest magnitudes and hence a difference is not seen as compared to the CFD-BEMT model. The CFD-BEMT TL shows the highest velocities in the outer wake region due to reduced reactive forces due to tip loss effect.

Figure 10 shows the variation of the average axial velocity with axial distance upstream and downstream of the wind turbine at TSR = 4 and TSR = 8. The first major observation is that, the higher the TSR, greater will be the reduction in average axial velocity from far upstream to far downstream. This is because at high TSRs, the axial momentum source terms and the axial loading are high, leading to a larger reduction in velocity. Secondly, the higher the axial source terms of a

CFD model, the larger will be the reduction in velocity from far upstream to far downstream. CFD-BEMT+LLT M3 model has the highest axial additional momentum source terms and hence shows the largest reduction in average axial velocity. CFD-BEMT TL has the lowest axial source terms and hence show the smallest reduction in average velocity.

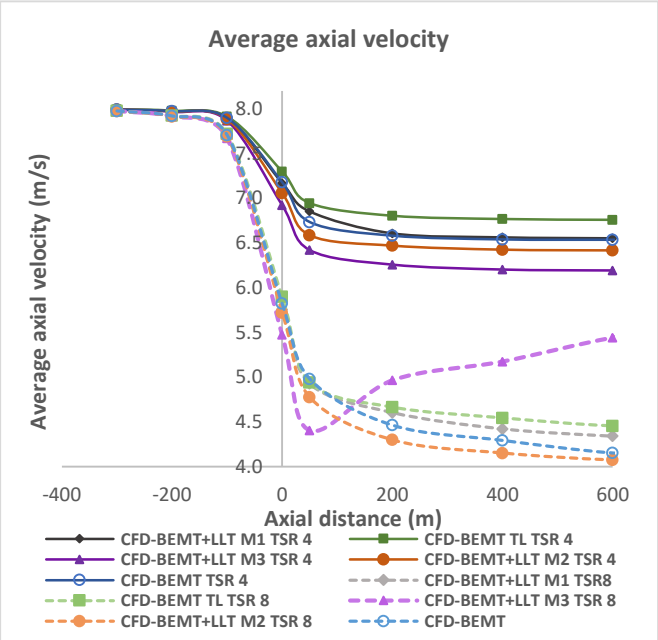

Figure10: Average axial velocity along axial distance

At TSR = 8, the CFD-BEMT+LLT M3 model shows the greatest reduction in average axial velocity until about 50 m downstream of turbine and then increases with the axial distance. This is because the CFD-BEMT+LLT M3 model at TSR = 8 generates turbulence at the downstream side of turbine. This turbulence causes mixing of the wake with the free stream air and hence recovers the velocity deficit in the wake.

6.4 Turbulence kinetic energy:

Figure 11 shows the plots of turbulence kinetic energy on xy plane for different CFD models and at different conditions. It is observed that only the CFD-BEMT+LLT M3 model with highest additional momentum source terms is capable of generating observable turbulence kinetic energy at higher TSRs (7, 8 and 9). High axial additional momentum source terms cause large reductions in axial velocity near the tip. A large reduction in axial velocity leads to strong shear effect between wake boundary and the free stream air which enhances turbulence. Turbulence causes mixing of the wake with the free stream air, which in turn recovers the velocity deficit in the wake. In wind farms, this turbulence is required at the downstream side of

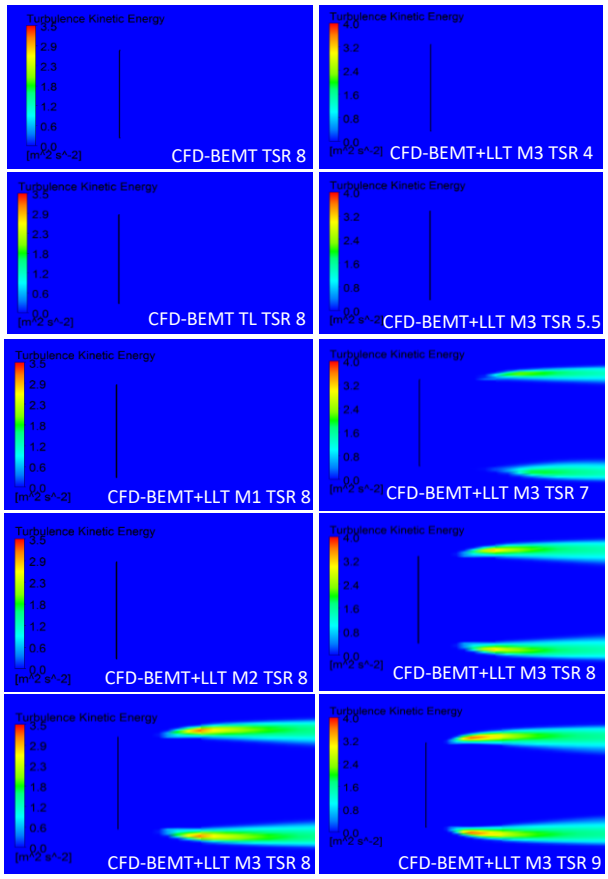

Figure 11: Turbulence kinetic energy plotted on xy-plane

wind turbines to recover velocity deficit in wakes so that more kinetic energy is available for downstream wind turbines. However, CFD-BEMT+LLT M3 is not a realistic model and there is a need of more realistic model that predicts the turbulence at the downstream side of wind turbines.

7. Conclusion:

The three enhanced actuator disc models show very different prediction of local flow field around the turbine at the tip region. Among the three

enhanced actuator disc models, for local flow field predictions, CFD-BEMT+LLT M1 model shows the worst correlation while CFD-BEMT+LLT M3 model shows the best correlation with the reference results obtained from LLT IST code. Flow field predictions with CFD-BEMT+LLT M1 is better than CFD-BEMT TL model but poorer than CFD-BEMT model.

CFD-BEMT+LLT M2 and CFD-BEMT+LLT M3 models show too high prediction in C_T as compared to reference results obtained from FAST BEMT and FAST BEMT with tip loss throughout the range of TSR presented which is clearly unrealistic. There is very narrow range of TSR, TSR = 5.5 to TSR = 7, where the C_P predicted by all the enhanced actuator disc models strongly correlate with the C_P predicted from FAST BEMT with tip loss. Outside that range, the enhanced actuator disc models will either under predict or over predict C_P. Among the three enhanced actuator disc models, for performance prediction, CFD-BEMT+LLT M1 model shows the best correlation while CFD-BEMT+LLT M3 model shows worst correlation with the reference results obtained from FAST BEMT with tip loss.

Only CFD-BEMT+LLT M3 model is capable of producing a noticeable turbulence level. Clearly, it can be seen that high source terms cause high reductions in axial velocities which lead to turbulence.

To conclude, it can be said that none of the enhanced actuator disc models is capable of accurately predicting performance and flow field simultaneously. Improvement in performance predictions occurs on the expense of faulty predictions of flow field and vice versa.

REFERENCES

1. Anderon, J. (2010). *Fundamentals of Aerodynamics* (5 ed.). McGraw-Hill Education.
2. Bai, C. -J., & Wang, W. -C. (2016). Review of computational and experimental approaches to analysis of aerodynamic performance in horizontal-axis wind turbines (HAWTs). *Renewable and Sustainable Energy Reviews, Volume 63*, 506-519.
3. Edmunds, M., Williams, A. J., Masters, I., & Croft, T. N. (2015). BEM-CFD: A Revised Model for Accurate Prediction. *Proceedings of the 11th European Wave and Tidal Energy Conference.* Nantes.
4. Esfahanian, V., Salavati Pour, A., Harsini, I., Haghani, A., Pasandeh, R., Shahbazi, A., & Ahmadi, G. (2013). Numerical analysis of flow field around NREL Phase II wind turbine by a hybrid CFD/BEM method. *Wind Engineering and Industrial Aerodynamics, 120*, 29-36.
5. Hansen, M. O. (2008). *Aerodynamics of Wind Turbines (Second Edition).* London: Earthscan.
6. Jonkman, J., Butterfield, S., Musial, W., & Scott, G. (2009). *Definition of a 5-MW Reference Wind Turbine for Offshore System Development.* National Renewable Energy Laboratory.
7. Manwell, J. F., Mcgowan, J. G., & Rogers, A. L. (2009). *Wind Energy Explained: Theory, Design and Application, 2nd Edition.* London: Wiley.
8. Mehta, D., van Zuijlen, A. H., Koren, B., Holierhoek, J. G., & Bijl, H. (2014). Large Eddy Simulation of wind farm aerodynamics: A review. *Wind Engineering and Industrial Aerodynamics*, 1-17.
9. Von Mises, R. (1959). *Theory of Flight.* Dover Publications.
10. Wu, Y. -T., & Porté-Agel, F. (2015). Modeling turbine wakes and power losses within a wind farm using LES: An application to the Horns Rev offshore wind farm. *Renewable Energy*, 945-955.
11. Jonkman, J., Butterfield, S., Musial, W., & Scott, G. (2009). Definition of a 5-MW Reference Wind Turbine for Offshore System Development. National Renewable Energy Laboratory.